Molecular Biology of the Cell

January 15, 2009
Volume 20
Number 2

www.molbiolcell.org

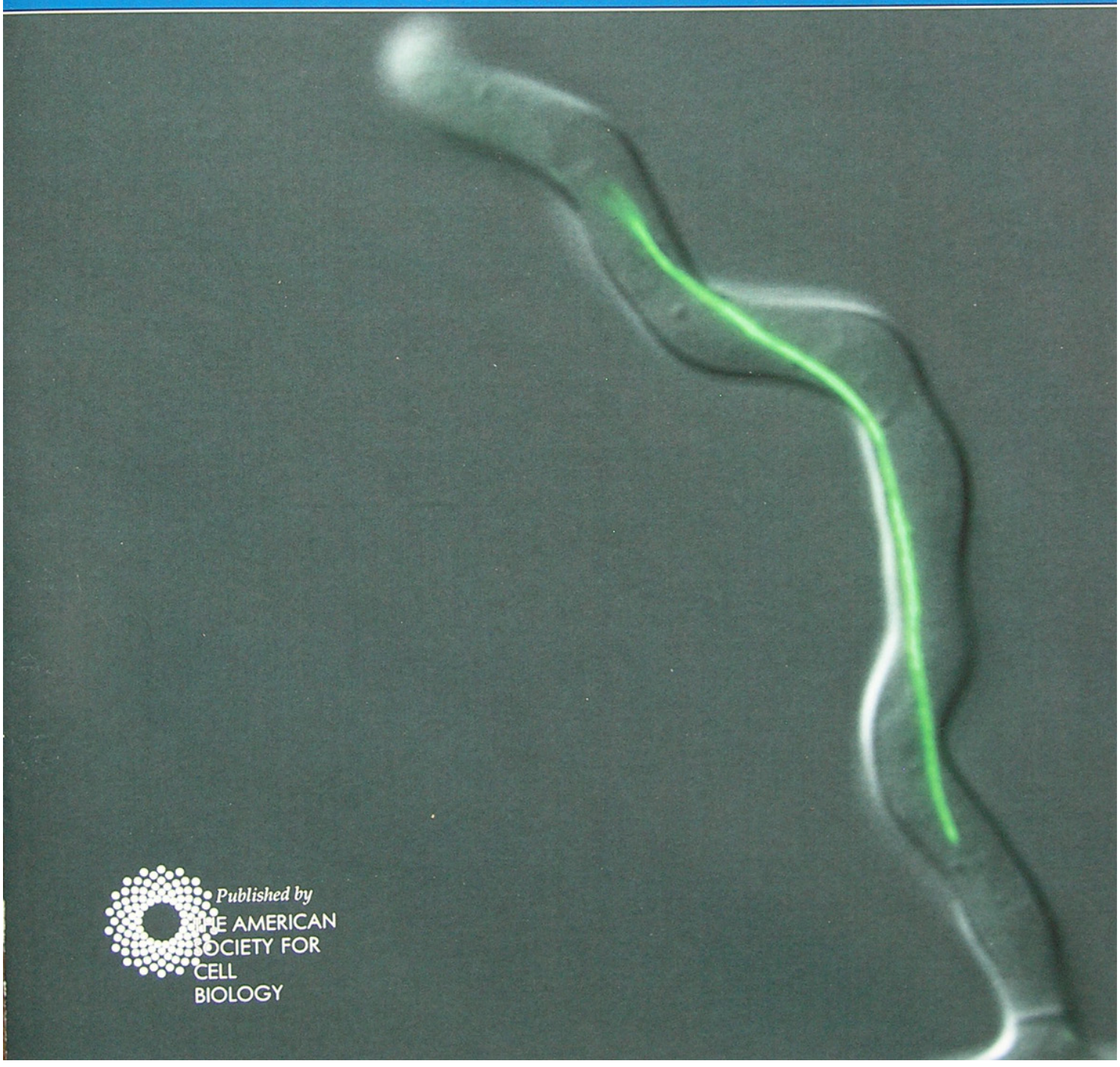

Published by
THE AMERICAN
SOCIETY FOR
CELL
BIOLOGY

Molecular Biology of the Cell
Vol. 20, 673–684, January 15, 2009

The *Aspergillus nidulans* Kinesin-3 UncA Motor Moves Vesicles along a Subpopulation of Microtubules

Nadine Zekert and Reinhard Fischer

University of Karlsruhe and Karlsruhe Institute of Technology, Institute of Applied Biosciences, Microbiology, D-76187 Karlsruhe, Germany

Submitted July 7, 2008; Revised October 14, 2008; Accepted November 14, 2008
Monitoring Editor: David G. Drubin

The extremely polarized growth form of filamentous fungi imposes a huge challenge on the cellular transport machinery, because proteins and lipids required for hyphal extension need to be continuously transported to the growing tip. Recently, it was shown that endocytosis is also important for hyphal growth. Here, we found that the *Aspergillus nidulans* kinesin-3 motor protein UncA transports vesicles and is required for fast hyphal extension. Most surprisingly, UncA-dependent vesicle movement occurred along a subpopulation of microtubules. Green fluorescent protein (GFP)-labeled UncA^{rigor} decorated a single microtubule, which remained intact during mitosis, whereas other cytoplasmic microtubules were depolymerized. Mitotic spindles were not labeled with GFP-UncA^{rigor} but reacted with a specific antibody against tyrosinated α-tubulin. Hence, UncA binds preferentially to detyrosinated microtubules. In contrast, kinesin-1 (conventional kinesin) and kinesin-7 (KipA) did not show a preference for certain microtubules. This is the first example for different microtubule subpopulations in filamentous fungi and the first example for the preference of a kinesin-3 motor for detyrosinated microtubules.

INTRODUCTION

The microtubule cytoskeleton in eukaryotic cells is essential for many dynamic processes. Among them are chromosome segregation, organelle movement, or the transportation of proteins, such as signaling complexes (Basu and Chang, 2007). These diverse functions are attributed not only to the inherent dynamic instability but also to the association with different molecular motor proteins, such as dynein and kinesin. Conventional kinesin is currently probably the best-studied molecular motor (Schliwa and Woehlke, 2003). ATP hydrolysis causes a small conformational change in a globular motor domain that is amplified and translated into movement with the aid of accessory structural motifs. Additional domains outside the motor unit are responsible for dimerization, regulation, and interactions with other molecules. The activity of conventional kinesin is required for exocytosis and thereby for fast fungal hyphal extension (Seiler *et al*., 1997; Requena *et al*., 2001).

Within the superfamily of kinesins, 17 families have been defined according to sequence similarities in the motor domain. One of these families is the Kif1/Unc-104 family, which has been renamed into the kinesin-3 family (Lawrence *et al*., 2004; Wickstead and Gull, 2006). This plus-end–directed motor harbors the motor domain in the N terminus (N-type), a pleckstrin homology (PH) domain for the binding of membranous cargoes at the C terminus and a forkhead-associated (FHA) domain (Klopfenstein *et al*., 2002). In contrast to the majority of dimeric kinesins, most Kin-3 kinesins are monomeric motors (Okada and Hirokawa, 1999, 2000), but a lysine-rich loop in KIF1A binds to the negatively charged C terminus of tubulin and compensates for the lack of a second heavy chain, allowing KIF1A to move processively like a dimeric motor (Okada and Hirokawa, 1999, 2000).

Unc-104 was first discovered in *Caenorhabditis elegans* shortly after the discovery of conventional kinesin (Otsuka *et al*., 1991). Mutations in *unc-104* caused uncoordinated and slow movement of corresponding mutants. The motor is required for synaptic vesicle transport (Hall and Hedgecock, 1991). Later, the motor was also discovered in mouse due to sequence similarities of cDNAs from a library of murine brain (Okada *et al*., 1995). The motor is associated with certain vesicles of the neuron, which transport synaptic vesicle proteins. The motor activity was measured in gliding assays and movement was measured at 1.2 μm/s, the fastest kinesin with anterograde movement at the time. It was observed that Kif1A apparently only binds to special vesicles and is only required for the anterograde transportation of certain synaptic proteins.

Although simple lower eukaryotes, e.g., *Saccharomyces cerevisiae*, serve as models for many cell biological phenomena, *S. cerevisiae* does not contain a member of the kinesin-3 family. However, this motor family was characterized in *Dictyostelium discoideum*, *Ustilago maydis*, *Neurospora crassa*, and *Thermomyces lanuginosus* (Pollock *et al*., 1999; Rivera *et al*., 2007). In *N. crassa*, one kinesin-3 motor, Kin2, is involved in mitochondrial distribution (Fuchs and Westermann, 2005). The kinesin-3 family contains also a unique fungal subgroup of "truncated" proteins, which do not have FHA and PH domains and may constitute a new subfamily (Schoch *et al*., 2003). Although the structure of the protein is very different from other kinesin-3 family members, it is very interesting that in *N. crassa* Kin3 can rescue the lack of Kin2 (Fuchs and Westermann, 2005).

In *U. maydis*, a kinesin-3 motor is required for endosome movement (Schuchardt *et al*., 2005; Steinberg, 2007). Deletion

This article was published online ahead of print in *MBC in Press* (http://www.molbiolcell.org/cgi/doi/10.1091/mbc.E08–07–0685) on November 26, 2008.

Address correspondence to: Reinhard Fischer (reinhard.fischer@kit.edu).

Table 1. *A. nidulans* strains used in this study

Strain	Genotype	Source
TN02A3	*pyrG89; argB2, nkuA::argB; pyroA4*	Nayak *et al.* (2006)
GR5	*pyrG89; wA3; pyroA4*	Waring *et al.* (1989)
RMS011	*pabaA1, yA2; argB::trpCΔB*	Stringer *et al.* (1991)
SJW02	*wA3; pyroA4; argB::trpCΔB; alcA(p)::GFP::tubA,* (GFP-MTs)	Toews *et al.* (2004)
SJW100	SJW02 transformed with pJH19, *pyroA4* (GFP-MT, DsRed labeled nuclei)	Toews *et al.* (2004)
SSK114	*wA3; pyroA4; alcA(p)::GFP::kipA-rigor* (GFP-KipA^{rigor})	Konzack *et al.* (2005)
SNR1	*yA2; argB::trpCΔB; pyroA4; ΔkinA::pyr4* (*kinA* deletion)	Requena *et al.* (2001)
AnKin26	*ΔkinA::pyrG, argB::trpCΔB; pyroA4*	Requena *et al.* (2001)
SNZ2	TN02A3 transformed with pAS3, *pyroA4* (GFP-UncA)	This study
SNZ3	TN02A3 transformed with pNZ5, *pyroA4* (*uncB* deletion)	This study
SNZ4	SNZ2 transformed with pJH19 (DsRed-stuA, GFP-UncA)	This study
SNZ8	TN02A3 transformed with pNZ9, *pyroA4* (mRFP1-UncA)	This study
SNZ9	TN02A3 transformed with pNZ13, *pyrG89* (*uncA* deletion)	This study
SNZ14	TN02A3 transformed with pNZ15, *pyroA4* (GFP-UncA^{rigor})	This study
SNZ15	SNZ3 crossed with RMS011, *pabaA1* (*uncB* deletion)	This study
SNZ26	SNZ8 crossed with SJW100, *pyroA4* (GFP-MT, mRFP1-UncA)	This study
SNZ27	SNZ9 crossed with RMS011, *pabaA1* (*uncA* deletion)	This study
SNZ29	SNZ9 crossed with SNZ15 (*uncA* and *uncB* double deletion)	This study
SNZ36	SNZ9 crossed with AnKin26 (*uncA* and *kinA* double deletion)	This study
SNZ54	TN02A3 transformed with pNZS20, *pyroA*4 (mRFP1-UncA^{rigor})	This study
SCS4-NZ	SNZ14 transformed with pCS5-NZ (GFP-UncA^{rigor}, mRFP1-KinA^{rigor})	This study
SCS5-NZ	TN02A3 transformed with pCS5-NZ, *pyrG89* (mRFP1-KinA^{rigor})	This study
SNZ63	SNZ9 crossed with XX60 (*uncA* and *nudA* double deletion strain)	This study
SNZ69	SNZ14 transformed with pNZ59 (GFP-UncA^{rigor}, mRFP1-TlgB)	This study
XX60	*nudA* deletion in GR5, *nudA*::*pyrG*	Xiang *et al.* (1995)
SNZ74	TN02A3 transformed with PNZ-SI49, *pyroA4* (*uncA*(P)-GFP-*uncA*)	This study

All strains harbor the *veA1* mutation.

of *kin-3* reduces endosome motility to 33% and abolishes endosome clustering at the distal cell pole and at septa. It was proposed that dynein and Unc104 counteract on endosomes to arrange them at opposing cell poles (Wedlich-Söldner *et al*., 2002). Schuchardt *et al*. (2005) also presented evidence that Kin3 is required for exocytosis, because acid phosphatase secretion was lowered to 50% in *kin-3* deletion strains.

In filamentous fungi it has been shown recently that not only exocytosis but also endocytosis is important for polarized growth (Araujo-Bazan *et al*., 2008; Fischer *et al*., 2008; Taheri-Talesh *et al*., 2008; Upadhyay and Shaw, 2008). However, no information was available on how endosomes are transported in *A. nidulans* or other filamentous fungi. In this study, two members of the kinesin-3 family were identified in *A. nidulans* and one of these members, UncA, was studied in detail. We present evidence that UncA is associated with endosomes and other vesicles and transports them surprisingly, along a subpopulation of microtubules.

MATERIALS AND METHODS

Strains, Plasmids, and Culture Conditions

Supplemented minimal (MM) and complete media (CM) for *A. nidulans* and standard strain construction procedures are described by Hill and Käfer (2001). A list of *A. nidulans* strains used in this study is given in Table 1 and Supplemental Table 1. Standard laboratory *Escherichia coli* strains (XL-1 blue, Top 10) were used. Plasmids are listed in Table 2 and Supplemental Table 2.

Molecular Techniques

Standard DNA transformation procedures were used for *A. nidulans* (Yelton *et al*., 1984) and *Escherichia coli* (Sambrook and Russel, 1999). For polymerase chain reaction (PCR) experiments, standard protocols were applied. DNA sequencing was done commercially (MWG Biotech, Ebersberg, Germany). Genomic DNA was extracted from *A. nidulans* with the DNeasy Plant Mini kit (QIAGEN, Hilden, Germany). DNA analyses (Southern hybridizations) were performed as described previously (Sambrook and Russel, 1999).

Deletion of uncA and uncB

The flanking regions of *uncA* were amplified by PCR using genomic DNA and the primers UncA-LB-fwd (5-CGTCGATGGAAGGCATATACTACTCGC-3) and UncA-LB-Sfi-rev (5-CGGCCATCTAGGCCGACAACAAATTGC-3) for the upstream region of *uncA* and UncA-RB-Sfi-fwd (5-CGGCCTGAGTGGCC-TCTATGTCTTCG-3) and UncA-RB-rev (5-CATCCACGTCCCCATAACTA-ATACCACC-3) for the downstream region. The fragments were cloned into pCR2.1-TOPO to generate pNZ7 and pNZ6, respectively. The SfiI restriction sites are underlined. In a three-fragment ligation, the *pyroA*-gene obtained from plasmid pNZ12 was ligated between the two *uncA*-flanking regions, resulting in vector pNZ13. The deletion cassette was amplified with the primers UncA-LB-fwd (5-CGTCGATGGAAGGCATATACTACTCGC-3) and UncA-RB-rev (5-CATCCACGTCCCCATAACTAATACCACC-3), and the resulting PCR product was transformed into the pyro-auxotrophic *A. nidulans* strain TN02A3.

The *uncB* flanking regions were amplified by PCR using genomic DNA and the primers uncB_LB_fwd (5-GGAAGTACACCTGCATGCTAATATCAT-CAG-3) and uncB_LB_Sfi_rev (5-CGGCCATCTAGGCCGCGGTGAAGTAT-AGAC-3) for the upstream region of *uncB* and uncB_RB_Sfi_fwd (5-CGGC-CTGAGTGGCCTGTTATGCGACGATG-3) and uncB_RB_rev (5-GACGAG-CAAGGGACGTGCCCTTCGGTG-3) for the downstream region and cloned into pCR2.1-TOPO, to generate pNZ3 and pNZ4, respectively. The restriction sites are underlined. The two *uncB*-flanking regions were ligated upstream and downstream of the *pyr4* marker in pCS1, generating pNZ5. This plasmid was cut with EcoRI and BglII, generating a fragment containing *pyr4* flanked by *uncB* sequences. This fragment was transformed into the uracil-auxotrophic strain TN02A3.

In each case, transformants were screened by PCR for the homologous integration event. Single integration of the construct was confirmed by Southern blotting (Supplemental Figure 1). One *uncA*- and one *uncB*-deletion strain were selected from the transformants and named SNZ9 and SNZ3, respectively. The coupling of the observed phenotypes with the gene-deletion events was confirmed by crosses and by down-regulation of the genes through the inducible *alcA* promoter (see below). A *uncA/uncB* double deletion strain was created by crossing the single *uncA* and *uncB* deletions generating SNZ29.

Tagging of Proteins with the Green Fluorescent Protein (GFP) and Monomeric Red Fluorescent Protein (mRFP) 1

To create an N-terminal GFP fusion construct of UncA, a 0.9-kb N-terminal fragment of *uncA* (starting from ATG) was amplified from genomic DNA,

Table 2. Plasmids used in this study

Plasmid	Construction	Source
pTN1	*pyroA* from *A. fumigatus*	Nayak *et al.* (2006)
pAS1	0.9-kb *uncA* fragment in pCR2.1-TOPO	This study
pAS3	0.9-kb *uncA* fragment in pCMB17apx	This study
pCR2.1-TOPO	Cloning vector	Invitrogen
pCS1	*N. crassa pyr-4* selectable marker as NotI fragment in pUMA208	Enke *et al.* (2007)
pCMB17apx	*alcA(p)::GFP*, for N-terminal fusion of GFP to proteins of interest; contains *N. crassa pyr4*	Efimov *et al.* (2006)
pDM8	GFP replaced mRFP1 in pCMB17apx	Veith *et al.* (2005)
pDC1	*argB* from *A. nidulans*	Aramayo *et al.* (1989)
pJH19	*gpd(p)::stuA(NLS)::DsRed* and *argB* as selectable marker	Toews *et al.* (2004)
pNZ1	1.6-kb *uncB* fragment with AscI and PacI sites in pCMB17apx	This study
pNZ3	1.0-kb 5-flanking region of *uncB* with SfiI site in pCR2.1-TOPO	This study
pNZ4	1.0-kb 3-flanking region of *uncB* with SfiI site in pCR2.1-TOPO	This study
pNZ5	*uncB*-deletion construct: flanking regions from pNZ3 and pNZ4 ligated with *pyr4* from pCS1	This study
pNZ6	1.0-kb 3-flanking region of *uncA* with SfiI site in pCR2.1-TOPO	This study
pNZ7	1.0-kb 5-flanking region of *uncA* with SfiI site in pCR2.1-TOPO	This study
pNZ8	*uncA*-deletion construct: flanking regions from pNZ6 and pNZ7 ligated with *pyr4* from pCS1	This study
pNZ9	GFP in pAS3 replaced with mRFP1	This study
pNZ11	1.7-kb *pyroA* fragment from pTN1 with NotI sites in pCR2.1-TOPO	This study
pNZ12	*pyr4* in pCS1 replaced with a 1.7-kb *pyroA* fragment from pNZ11	This study
pNZ13	*uncA*-deletion construct: *pyr4* in pNZ8 replaced with *pyroA* from pNZ12	This study
pNZ15	pAS3 mutagenesis to introduce the G116E mutation in the p-loop of UncA, ($UncA^{rigor}$)	This study
pNZS20	GFP in pNZ15 replaced with mRFP1	This study
pCS1-NZ	1.3-kb *kinA* fragment in pCR2.1-TOPO	This study
pCS2-NZ	1.3-kb *kinA* fragment in pCMB17apx, *pyr4* replaced with *pyroA*	This study
pCS3-NZ	1.3-kb *kinA* fragment in pDM6, *pyr4* replaced with *pyroA*	This study
pCS4-NZ	pCS2-NZ mutagenesis to introduce the G97E mutation in the p-loop of KinA, ($KinA^{rigor}$)	This study
pCS5-NZ	GFP in pCS4-NZ replaces with mRFP1	This study
pNZ-SI49	1.5-kb *uncA*(p) fragment in pAS3 with KpnI-EcoRI sites	This study
pNZ54	TlgB ORF fragment in pCR2.1-TOPO	This study
pNZ58	TlgB ORF fragment from pNZ54 in pCMB17apx, *pyroA4* instead of *pyr4* as marker	This study
pNZ59	GFP in pNZ58 (mRFP1-TlgB) replaced with mRFP1	This study

with the primers uncA_Asc_fwd1 (5-GGGCGCGCCCGGCATGGCGCCAGGAGGTGGTG-3) and uncA_Pac_rev1 (5-CTTAATTAAACCTAGCACCGGTGGCTCCAGTCG-3) and cloned into pCR2.1-TOPO, yielding pAS1. The restriction sites are underlined. The AscI-PacI fragment from pAS1 was subcloned into the corresponding sites of pCMB17apx, yielding pAS3. To create an N-terminal mRFP1 fusion construct of UncA, the GFP KpnI-AscI fragment from pAS3 was substituted by mRFP1 from pDM8, yielding pNZ9. To produce UncA N-terminally tagged with GFP under the native promoter, a 1.5-kb fragment of the putative *uncA* promoter was amplified from genomic DNA with the primers UncA nat(P) EcoRI fwd (5-GGA ATT CTC ATC ACC TAC TGG AGG CGC GC-3) and UncA nat(P) KpnI rev (5-CGG TAC CTT TGG CCT ATA GCC CAT ACA CC-3), digested with EcoRI and KpnI, and the two fragments were ligated with EcoRI-KpnI–digested pAS3, yielding pNZ-SI49 (*alcA* promoter replaced with the *uncA* promoter in pAS3).

Using the same approach as for UncA, N-terminal GFP fusion constructs of KinA and TlgB were created. The primer set used for KinA was KinA ATG AscI fwd (5-GGG CGC GCC CGG CAT GGC GTC CTC TAC-3) and KinA 1324bp Pac rev (5-CTT AAT TAA CAA GAA CGA TGC TGG GTG TGC-3). The PCR fragment was cloned into pCR2.1-TOPO and subsequently into pCMB17apx (*pyroA* as selection marker), yielding plasmid pCS2-NZ. The primer set used for TlgB was Tlg2nidulansAscI fwd (5-GGG CGC GCC CGG CAT GTG GCG GGA CCG-3) Tlg2nidulansPacI rev (5-CTT AAT TAA CTA CGG GGC AAC GAT GCG GCC-3). The PCR fragment was cloned into pCR2.1-TOPO and subsequently into pDM8 (*pyroA* as selection marker), yielding pNZ58. All plasmids were transformed into the uracil- and pyrodoxin-auxotrophic strain TN02A3 (Δ*nkuA*). The integration events were confirmed by PCR and Southern blotting and microscopy (data not shown).

Creation of an $uncA^{rigor}$ and $kinA^{rigor}$ Mutant Allele

We changed the glycine residue 116 to glutamate by site-directed mutagenesis by using the oligonucleotides UncA P-Loop Gly fwd (5-GGT CAG ACC GGT TCG GAG AAG TCT TAC TCG-3) and UncA P-Loop Gly rev (5-CGAGTAAGACTTCTCCGAACCGGTCTGACC-3), plasmid pAS3 as template, and the QuikChange XL site-directed mutagenesis kit (Stratagene, Heidelberg, Germany); this yielded plasmid pNZ15. We transformed strain TN02A3 and searched for transformants in which pNZ15 was homologously integrated at the *uncA* locus. Among 12 transformants, two (1 transformant named SNZ14) displayed the *uncA* deletion phenotype under both repressing and inducing conditions. PCR and Southern blot analysis confirmed that the construct was integrated at the *uncA* locus in both transformants. The PCR fragments were sequenced to confirm the mutagenesis event.

The same was done for *kinA* using primer KinA Rigor P-Loop for (5-C GGT CAA ACC GGT GCA GAG AAG TCG TAT AC-3) and KinA Rigor P-Loop rev (5-GT ATA CGA CTT CTC TGC ACC GGT TTG ACC G-3) to change glycine residue 97 to glutamate using pCS2-NZ as template.

Light and Fluorescence Microscopy

For live-cell imaging of germlings and young hyphae, cells were grown on coverslips in 0.5 ml of MM 2% glycerol (derepression of the *alcA* promoter, moderate induction) or MM 2% glucose (repression of the *alcA* promoter). Cells were incubated at room temperature for 1–2 d. For pictures of young hyphae of each strain, the spores were inoculated on microscope slides coated with MM 2% glucose 0.8% agarose and grown at 30°C for 1 d. Images were captured at room temperature (200-ms exposure time) using an Axio Imager Z1 microscope (Carl Zeiss, Jena, Germany). Images were collected and analyzed with the AxioVision system (Carl Zeiss). Dynamic processes in the hyphae were quantified using the same software analyzing series of single pictures. We also used an SP5 laser scanning microscope (Lecia, Wetzlar, Germany).

N-[3-Triethylammoniumpropyl]-4-[p-diethylaminophenylhexatrienyl] Pyridinium Dibromide (FM4-64), Benomyl, and Cytochalasin A Treatment

FM4-64 was used at a concentration of 10 μM in the medium. Coverslips were incubated for 1–2 min and washed. Methyl 1-(butylcarbamoyl)-2-benzimidazole carbamate (benomyl; Aldrich Chemical, Milwaukee, WI) was used at a final concentration of 2.5 μg/ml in the medium from a stock solution of 1 mg/ml in ethanol. Cytochalasin A (Sigma Chemie, Deisenhofen, Germany) was used at a final concentration of 2 μg/ml in the medium from a stock solution of 100 mg/ml in dimethyl sulfoxide.

Immunostaining

We inoculated 10^3 spores/ml with 0.5 ml MM on sterile coverslips for 12–24 h at room temperature (RT). Cells were fixed for 30 min with formaldehyde and digested for 1 h by using digestion solution (GlucanX; β-D-glucanase, zymolyase, and driselase in Na-phosphate buffer with 50% egg white),

washed with phosphate buffered saline (PBS), incubated in −20°C methanol for 10 min before and blocked with TBST + 5% skim milk before incubation with the first antibodies (anti-tubulin, 1:500) in Tris-buffered saline/Tween 20 (TBST) overnight at 4°C. Next, cells were washed and incubated with the secondary antibodies (1:200 in TBST) for 1 h at RT. Cells were washed and mounted on microscope slides (with mounting media with 4,6-diamidino-2-phenylindole [DAPI] and VECTORSHIELD [Vector Laboratories, Burlingame, CA]), sealed with nail polish, and stored at 4°C overnight in the dark before doing the microscopy. As monoclonal anti-α tubulin antibodies, we used the following clones from Sigma Aldrich: DM1A (anti-α tubulin), B3 (anti-polyglutamylated tubulin), 6–11B-1 (anti-acetylated tubulin), and TUB-1A2 (anti-tyrosinated tubulin). As secondary antibodies, we used fluorescein isothiocyanate (FITC)-conjugated anti-mouse immunoglobulin G (IgG) (Fab-specific) (Sigma Chemie), FITC-conjugated anti-mouse IgG (whole molecule) (Sigma Chemie), and Cy3 conjugated AffiniPure goat anti-mouse IgG (H+L) (Dianova, Hamburg, Germany).

RESULTS

Isolation of UncA and UncB

We identified eleven different kinesins in *A. nidulans*, with two members (named UncA and UncB) of the kinesin-3 family (formerly called *unc-104* family) (Rischitor *et al*., 2004; Galagan *et al*., 2005). The predicted structure of the *uncA* and the *uncB* genes were confirmed through amplification of small cDNAs and subsequent sequencing. The *uncA* gene contains an intron of 75 base pairs located between amino acid 21 and 22 of the open reading frame. The UncA protein is comprised of 1631 amino acids, with a calculated molecular mass of 182.7 kDa. The predicted motor domain starts two amino acids downstream of the initiation codon and consists of 361 amino acids. The ATP-binding motif (P-loop) starts at amino acid 111 (GQTGSGKS). The C-terminal half of the motor domain displays the highly conserved regions termed switch I (NETSSR), at amino acid position 224 and switch II (DLAGSE), at amino acid position 261, which are involved in nucleotide binding (ATP). Two microtubule-binding motifs were found, MT1 (RDLL) starting at amino acid position 170 and MT2 (VPYRDS) starting at amino acid position 312 (Song *et al*., 2001).

Comparison of UncA with other Kin-3 proteins revealed 60% homology with *N. crassa* Nkin2, 48.1% with *U. maydis*, and 46.5% with *C. elegans* Unc104, but 80.8% homology with *Aspergillus oryzae*, and 88.1% with *Aspergillus fumigatus* (Figure 1). The homology between the proteins is much higher in the motor domains (Supplemental Figure 2). The C terminus of UncA exhibited very low sequence similarity to the corresponding regions of other Kin-3 family proteins, besides a forkhead-associated (FHA) domain at amino acid 496–596 and a pleckstrin homology (PH) domain at amino acid 1509–1615. The PH domain has been reported previously in Unc104-related kinesins in *C. elegans* where it has been proposed to bind lipids and lipid rafts to dock onto membrane cargoes (Klopfenstein *et al*., 2002). The FHA domain is proposed to be involved in signaling and protein–protein interactions of kinesins (Westerholm-Parvinen *et al*., 2000). In addition, a novel role for the FHA domain in the regulation of kinesin motors was discovered previously (Lee *et al*., 2004).

The *uncB* gene contains an intron of 52 base pairs at position 112 of the open reading frame. The derived UncB protein is composed of 671 amino acids, with a calculated molecular mass of 75 kDa. The motor domain starts 116 amino acids downstream of the initiation codon and consists of 356 amino acids. The P-loop starts at amino acid 212 (GQTGSGKS). The C-terminal half of the motor domain displays the highly conserved regions termed switch I (NDTSSR), at amino acid 326 and switch II (DLAGSE) at amino acid 363, which are involved in nucleotide binding (ATP). Two microtubule-binding motifs were found, MT1 (RDLL) at amino acid position 268 and MT2 (VPYRDS) at amino acid 417 (Figure 1).

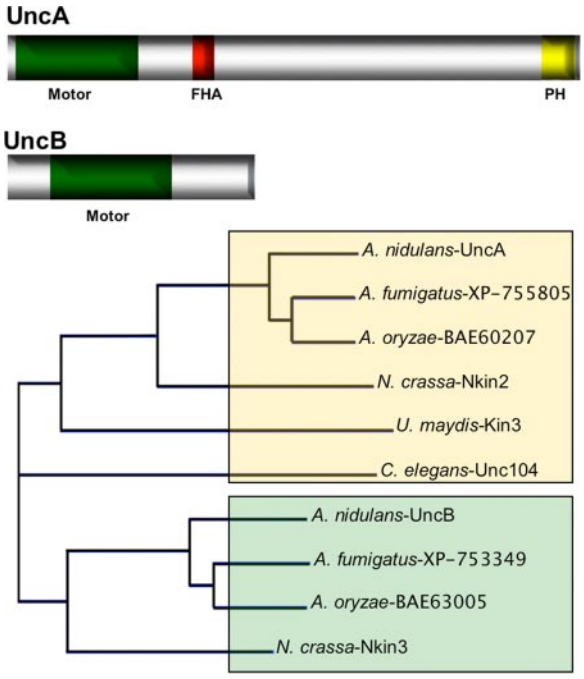

Figure 1. Scheme of UncA and UncB and relatedness analysis with other kinesins of the kinesin-3 family. The UncA (1631 amino acids) and UncB (671 amino acids) protein sequences were analyzed with SMART (http://smart.embl-heidelberg.de) and besides the kinesin motor domains a FHA and a PH domain were identified in UncA. The relatedness analysis was done with Vector NTI by using standard parameters. UncB groups with the fungal-specific subclass as indicated by green shading.

Comparison of full-length UncB with other Kin-3 proteins revealed 56.4% homology with *N. crassa* Nkin3, 83% with *A. oryzae*, and 75% with *A. fumigatus*. The N-terminal region starts with a short nonmotor sequence of 104 amino acids (Figure 1). The 195 amino acid-long part outside the motor domain exhibits very low sequence similarity to the corresponding regions of related proteins.

Deletion of uncA and uncB

We deleted the *uncA* open reading frame in strain *TN02A3* with *pyroA* as selection marker and confirmed the deletion event by diagnostic PCR (data not shown) and Southern blot (Figure 2 and Supplemental Figure 1). One of the strains (SNZ9) was used for further analysis and the construction of *uncA*-deletion strains in other genetic backgrounds. Colonies of this strain grew slower than wild-type colonies and seemed more compact. When we compared the distribution of nuclei or mitochondria, or the organization of the microtubule cytoskeleton, we did not observe any difference to wild-type (Supplemental Figure 3). However, we noticed more branching in the Δ*uncA* strain. At higher temperature, we observed a slight curved hyphal phenotype similar to the phenotype of cell end marker mutants (Takeshita *et al*., 2008) (Figure 2B).

We deleted the *uncB* open reading frame in strain *TN02A3* with *pyr4* as selection marker and confirmed the deletion event by diagnostic PCR (data not shown) and Southern blot (Figure 2A and Supplemental Figure 1). One of the strains (SNZ3) was used for further analysis and the construction of

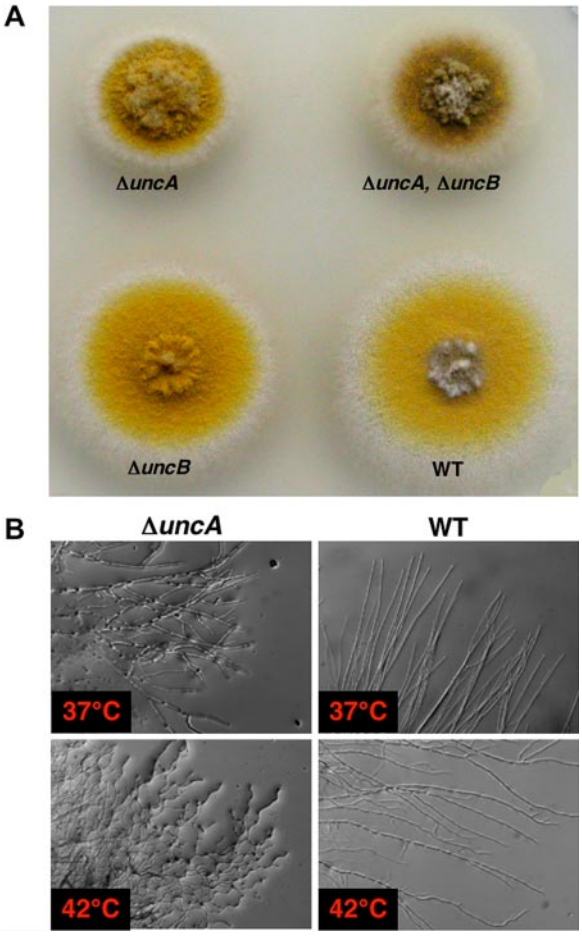

Figure 2. Phenotype of an *uncA*, an *uncB*, and a double-deletion strain. (A) Growth of the strains SNZ27 (Δ*uncA*), SNZ15 (Δ*uncB*), SNZ29 (Δ*uncA*, Δ*uncB*), and RMS011 on minimal medium for 3 d at 37°C. (B) Hyphal growth of the *uncA*-deletion strain and the wild type at 37 and 42°C grown on glycerol minimal medium for 2 d.

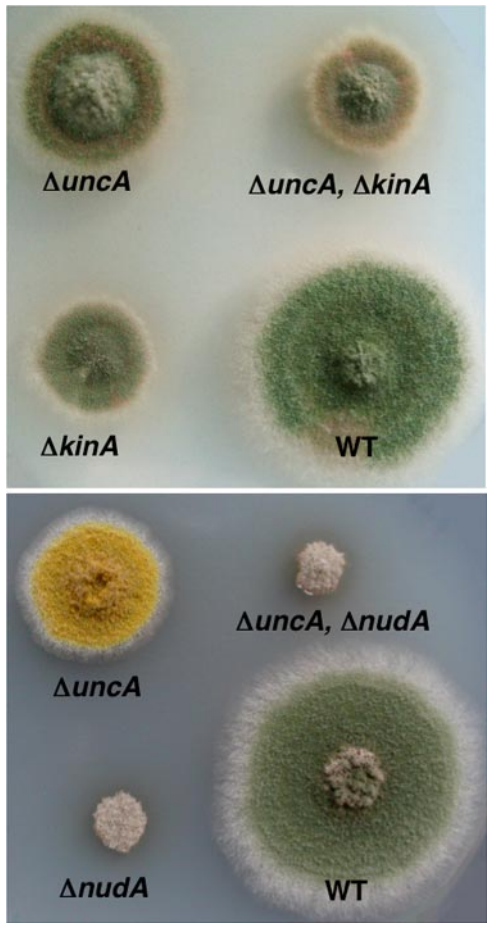

Figure 3. Comparison of colony growth of different mutants as labeled. Top, deletion strains of *uncA* (SNZ9) and conventional kinesin *kinA* (AnKin26) in comparison with the double deletion strain (SNZ36) and a wild type (TN02A3). Bottom, comparison of the colony phenotypes of the *uncA*-deletion strain (SNZ27) and the dynein-deletion strain (*nudA*) (XX60) and the corresponding double deletion (SNZ63). Colonies were grown for 3 d on glucose minimal medium at 37°C.

uncB-deletion strains in other genetic backgrounds. Colonies of this strain grew like wild-type colonies. We did not observe any difference to wild type with respect to nuclear or mitochondrial distribution, septum formation, or branching (data not shown).

To investigate whether UncA and UncB are functionally related, we constructed an *uncA/uncB* double deletion mutant (Figure 2A). It displayed the same compact growth phenotype than the *uncA*-deletion mutant. The analysis of nuclear and mitochondrial distribution, the organization of the microtubule (MT) cytoskeleton revealed no difference in comparison with the wild type (Suelmann and Fischer, 2000). This was unlike the situation in *N. crassa* (Fuchs and Westermann, 2005). Our results suggested that UncA and UncB act in different pathways. Therefore, we focused in this paper only on the molecular analysis of UncA.

To test whether deletion of *uncA* causes a more severe phenotype in the absence of other motor proteins involved in polarized growth, we constructed an *uncA/kinA* (conventional kinesin) and an *uncA/nudA* (heavy chain of dynein) double-deletion mutant (Figure 3). The growth defects of these strains were comparable to the growth defect of stains with single mutations in either *kinA* or *nudA*, respectively.

Localization of UncA along Microtubules

The UncA protein was visualized by fusion with a fluorescent protein (GFP or mRFP1 in the vector pMCB17apx). A 0.9-kb fragment from the *uncA* 5′-end was fused to GFP and under the control of the *alcA*-promoter (de-repressed with glycerol, induced with threonine, repressed with glucose). After homologous integration of the construct at the *uncA* locus, the 0.9-kb fragment becomes duplicated and the full-length *uncA*-open reading frame is fused to GFP and is under the control of the *alcA* promoter. The *uncA-GFP* strain (SNZ2), in which plasmid pAS3 is homologously integrated, grew like the *uncA*-deletion strain when grown on glucose medium and like wild type when grown on glycerol or threonine medium, showing that the GFP fusion protein was fully functional (Supplemental Figure 4). Under inducing conditions, GFP was visible as fast-moving spots and accumulated sometimes at the tips of the hyphae (Figure 4A and Supplemental Movie 1). They moved into two directions with speeds of up to 4 μm s^{-1}. The speed was determined as described in *Materials and Methods*. The GFP signal at the tip looked like an accumulation of dynamic vesicles. After addition of the microtubule-destabilizing drug benomyl,

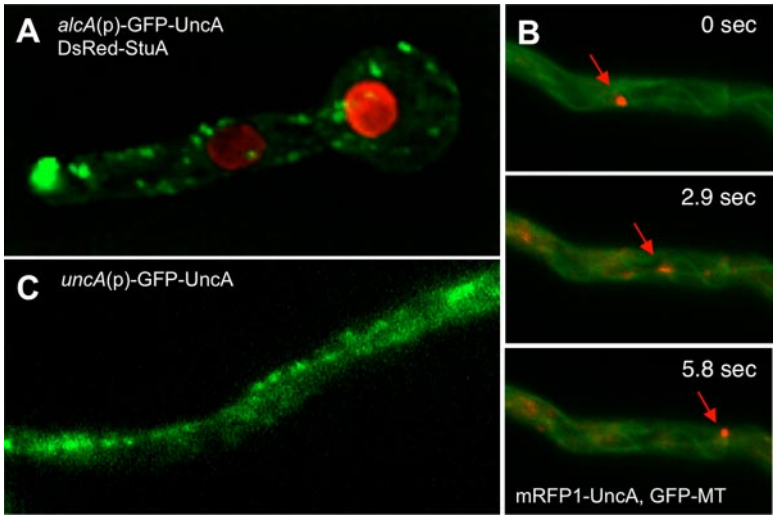

Figure 4. Localization of UncA. (A) UncA was labeled with GFP and nuclei with DsRed. UncA was under the control of the *alcA* promoter (SNZ4). (B) Movement of UncA along microtubules. Time-lapse analysis of mRFP1-UncA in a strain with GFP tagged microtubules (SNZ26). One spot (indicated with the arrow) was focused and followed over time. The time between the exposures of the pictures is indicated. (C) GFP-UncA expressed under the natural promoter (SNZ74). A pearl-string like arrangement of the signal is visible.

vesicle movement in the hyphae and at the tip stopped (Supplemental Figure 5), suggesting microtubule-dependent movement. This finding was supported by colocalization of GFP-labeled microtubules with mRFP1-labeled UncA (Figure 4B and Supplemental Movie 2). To exclude the possibility that the observed localization was due to *alcA*-driven expression (glycerol as carbon source) of the GFP-UncA fusion protein, we replaced the *alcA* promoter with a 1.5-kb DNA fragment derived from the region upstream of the *uncA* start codon. This construct was transformed into TN02A3. One strain with a homologous integration event at the *uncA* locus was selected for further analysis (SNZ74) (Supplemental Figure 6). The strain seemed like wild type, suggesting functionality of the GFP-UncA fusion protein. Although the GFP signal was weaker than in the previous strains, small moving spots were clearly visible (Figure 4C). These results suggested that in the above-described experiments *alcA*-driven expression with glycerol in the medium did not cause artifacts and/or mislocalization of the protein. Interestingly, the GFP-UncA protein preferred essentially one track in the cell (Supplemental Movie 1). This suggested a preference of UncA for a certain class of microtubules.

UncA Is Involved in Vesicle Transport

Because we excluded a role of UncA in mitochondrial movement (Supplemental Figure 7) and because Kin-3 of *U. maydis* localizes to early endosomes, we analyzed the association of UncA with vesicles. To this end, we stained the plasma membrane in *A. nidulans* strain (SNZ74, *uncA(p)::GFP::uncA*) with FM4-64. After internalization of the membrane, early endosomes were visible. The movement of the corresponding vesicles resembled the movement of GFP-UncA (Supplemental Movie 3). However, colocalization of the red FM4-64 and the green GFP signal proved to be difficult because of the high speed of the structures. This technical obstacle was overcome by generating a rigor variant of UncA by changing glycine residue 116 to a glutamate (see *Materials and Methods*). This modification of the P-loop allows binding of the motor to the microtubules but not their dissociation (Meluh and Rose, 1990; Nakata and Hirokawa, 1995). The movement of FM4-64–labeled vesicles was reduced and colocalization with GFP-UncA^{rigor} was observed in some cases (Figure 5A). Quantification was impossible, because of the alignment of the vesicles to a continuous structure (see below). That not all GFP signals colocalized with FM4-64 suggests that UncA is not only associated with early endosomes but also with other vesicles. As a further proof for the binding of UncA to endosomes, we tagged a *S. cerevisiae* Tlg2 homologue, named TlgB in *A. nidulans*, with mRFP1 (see *Materials and Methods*). This protein was used before for endosome labeling in *A. oryzae* (Kuratsu *et al.*, 2007). TlgB (317 amino acids) displays 39.9% homology to

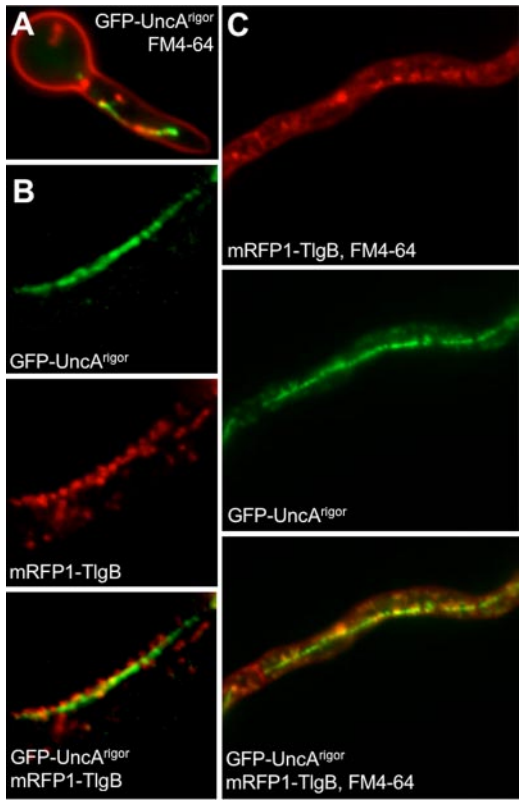

Figure 5. Colocalization of endosomes with UncA. (A) Endosomes were visualized with FM4-64 and UncA^{rigor} with GFP (SNZ14). UncA^{rigor} was expressed from the *alcA* promoter in the presence of glycerol. (B) Colocalization of mRFP1-TlgB and GFP-UncA^{rigor} (SNZ69). (C) Colocalization of mRFP1-TlgB and FM4-64 with GFP-UncA^{rigor}.

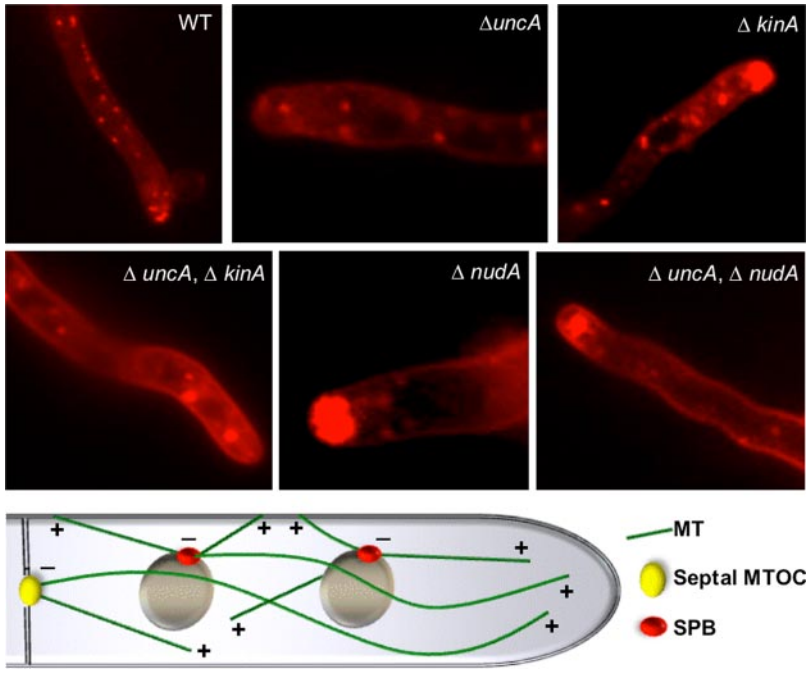

Figure 6. FM4-64 staining in the strains indicated in the pictures and scheme of microtubule organization in the hyphal tip of *A. nidulans*. The strains were the same as described in the legend for Figure 4. FM4-64 staining was done as described in *Materials and Methods*. The mixed polarity of MTs indicated in the scheme will be discussed in the first chapter of the Discussion section.

the *S. cerevisiae* Tlg2 protein (398 amino acids). Both proteins share a Syntaxin and target-soluble *N*-ethylmaleimide-sensitive factor attachment protein receptor domain. To localize TlgB, we cloned the full-length coding region downstream of mRFP1 in the vector pDM8 and integrated it ectopically into the genome of SNZ14 (GFP-UncA^{rigor})(SNZ69). Southern blot analysis showed that the strain contained several integrations. Fluorescence microscopy revealed partial colocalization between UncA-GFP and mRFP1-TlgB (Figure 5B). Three other strains, also with integrations at different places in the genome, showed the same localization pattern, indicating that the localization was independent of the integration site. Strain SNZ69 was treated with FM4-64. Because in *S. cerevisiae* Tlg1 and Tlg2 endocytic vesicles were only transiently labeled with FM4-64 (Holthuis *et al*., 1998), we anticipated that the combination of FM4-64 and mRFP1-TlgB would stain all GFP-UncA^{rigor}–labeled vesicles (Figure 5C). Indeed we detected more colocalization, but still some GFP signals did not localize at the same places as the red signals, again indicating that UncA is associated not only with endosomes.

To study whether the observed movement of FM4-64–labeled vesicles was due to UncA or another motor activity, we studied vesicle behavior (stained with FM4-64) in *uncA*-, *kinA*-, and *nudA*-deletion strains (Figure 6 and Supplemental Movies 4–8). It was clearly visible that the movement changed dramatically when UncA or dynein were absent or nonfunctional, respectively. Long-distance movement as observed in wild type was largely reduced in 28 out of 37 hyphae. In nine hyphae, one or two vesicles were observed moving long distances (2-min observation time). In addition to the reduced motility, an accumulation of vesicles was observed in the dynein mutant at the hyphal tip, suggesting that dynein is required for retrograde transportation. In the double mutant Δ*nudA*/Δ*uncA* the defect in vesicle movement was the same as in the dynein single mutant. In the *kinA*-deletion strain, long-distance vesicle movement occurred, and a vesicle accumulation was visible at the hyphal tip. The effect was not as strong as in the dynein mutant. This observation can be explained by the accumulation of dynein at the microtubule plus end, and thereby the transportation to the tip zone, depending on conventional kinesin (Zhang *et al*., 2003). Hence, the observed defect of vesicle movement in the *kinA* mutant is probably due to the lack of dynein at the tip. A double mutant between Δ*kinA* and Δ*uncA* displayed a similar phenotype as the Δ*uncA*-deletion strain, with some more accumulated vesicles at the tip (Figure 6).

UncA Localizes to a Subpopulation of Microtubules

In the above-described experiments, we found that a rigor mutation in the UncA motor reduced the movement of the vesicles, and most surprisingly, the GFP-UncA signal was aligned along a rod-like structure in the cell (Figure 7, A and B). This rod was a microtubule, as shown by disassembly with benomyl (Supplemental Figure 7). To analyze this phenomenon further, we stained the microtubules by secondary immunofluorescence by using anti-α-tubulin antibodies and compared them with the observed rod structure stained with mRFP1-UncA. Indeed, the red rod represented a subpopulation of microtubules (Figure 7C). Because UncA seemed to be a nice marker for this population of microtubules, we analyzed the occurrence in different developmental stages. We found the GFP-UncA labeled rod-like structures already in conidiospores, as well as in young germ tubes and older hyphal compartments. This suggests that the occurrence of this microtubule population is independent of the growth phase of the hyphae. In addition, we observed this rod during mitosis. In contrast, mitotic spindle microtubules were not labeled with mRFP1-UncA^{rigor} (Figure 8A). This suggests that UncA associates with the more stable cytoplasmic microtubules. This is in agreement with previous observations that not all microtubules are disassembled during nuclear division and are thus of different stability (Veith *et al*., 2005).

To analyze the observed specificity of the UncA motor protein, we studied the presence of posttranslational modifications of tubulin in *A. nidulans*. One modification is the addition of glutamate residues near the carboxy terminus of α- and β-tubulin. Using anti-polyglutamylated tubulin anti-

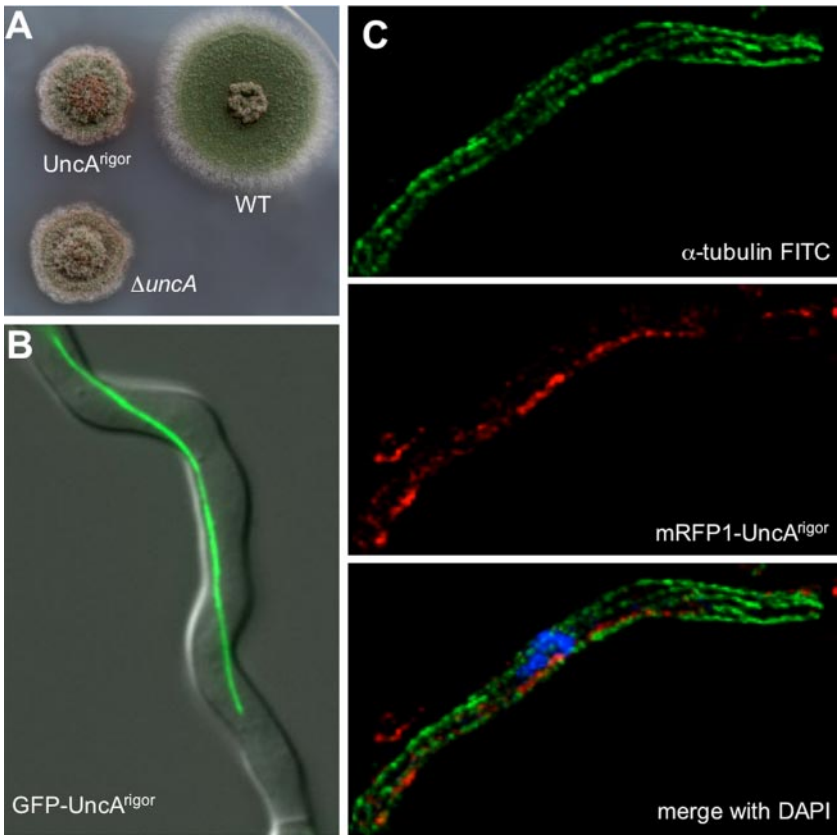

Figure 7. Localization of UncA^{rigor} along a single microtubule. (A) The colony of an *uncA^{rigor}* mutant (SNZ14) shows the same phenotype as an *uncA*-deletion strain (SNZ9). (B) GFP-UncA^{rigor} localizes to a rod-like structure in a hyphal compartment. (C) Immunostaining of a tip compartment of an mRFP1-UncA^{rigor} strain (SNZ54) with anti-α-tubulin antibodies and FITC-labeled secondary antibodies. Nuclei were stained with DAPI. Top, FITC fluorescence. Middle, mRFP1 fluorescence. Bottom, overlay with the DAPI channel.

bodies for immunostain experiments, we were not able to visualize microtubules (data not shown). It is possible, that these antibodies do not recognize the *A. nidulans* modified tubulin. However, it is also possible that this modification does not exist in *A. nidulans*. The same was true for the analysis of acetylated microtubules (data not shown). Another modification is a reversible removal of a terminal tyrosin residue of α-tubulin. In *A. nidulans* the C terminus of α-tubulin ends with the amino acids valin, glutamate, and tyrosine. We used monoclonal anti-tyrosine tubulin antibodies against the tyrosinated form of α-tubulin. These antibodies stained cytoplasmic and mitotic microtubules (Figure 8). In interphase cells, all microtubules were stained with the antibody, including the microtubule characterized by mRFP1-UncA^{rigor} (Figure 8B). However, when we looked at mitotic cells, the mRFP1-UncA^{rigor} rod was clearly visible and was not stained with the anti-tyrosin tubulin antibody (Figure 8A). In comparison, the mitotic spindle was stained. These findings suggest that UncA binds preferentially to detyrosinated microtubules. In interphase cells, tyrosinated and detyrosinated microtubules seem to exist in parallel in one microtubule bundle. During mitosis the tyrosinated cytoplasmic microtubule depolymerizes and the detyrosinated ones remain.

To test whether the observed behavior of the UncA^{rigor} motor protein is specific for UncA, we compared the results to the binding of kinesin rigor variants of kinesin-1 (conventional kinesin, KinA) and kinesin-7 (KipA) (Seiler *et al*., 1997; Requena *et al*., 2001; Konzack *et al*., 2005) (Figure 9). Kinesin-8 (KipB) was already studied in a previous article (Rischitor *et al*., 2004) and did not show a preference for certain microtubules (Supplemental Figure 6). In KipA and KinA, we did not find any specificity either. Comparison of KinA^{rigor} with UncA^{rigor} localization confirmed the specificity of UncA (Figure 9C). During our experiments, we made another interesting observation. We noticed that KinA^{rigor} did not decorate microtubules, stained with the anti-tyrosin tubulin antibody, at the very tip of the hypha (Figure 9D).

DISCUSSION

In this article, we show that UncA is required for vesicle movement in *A. nidulans* and found that their transportation preferably occurs along a subpopulation of microtubules. This is in contrast to the finding in *N. crassa*, where this motor protein transports mitochondria (Fuchs and Westermann, 2005), but in agreement with our previous finding that in *A. nidulans* mitochondrial movement depends on the actin cytoskeleton (Suelmann and Fischer, 2000). We showed here that vesicle movement was dependent on the motor activity of UncA and occurred into both directions in the cell. This bidirectional movement and the accumulation of vesicles in the tip compartment of a dynein and a conventional kinesin mutant, is comparable with the situation in *U. maydis* and can be explained if UncA and dynein transport these vesicles into opposite directions, UncA toward the plus and dynein toward the minus end of microtubules (Wedlich-Söldner *et al*., 2002). The lack of one motor causes an imbalance of the forces and an accumulation of the vesicles. However, first it was surprising that the vesicles only accumulated in the dynein mutant and not in the rear of the hypha in the *uncA*-deletion strain. To explain this, it has to be considered that in the tip compartment almost all microtubules are oriented with their plus ends toward the growing tip. In regions behind the first nucleus, however, the orientation is mixed and thus a single motor can transport

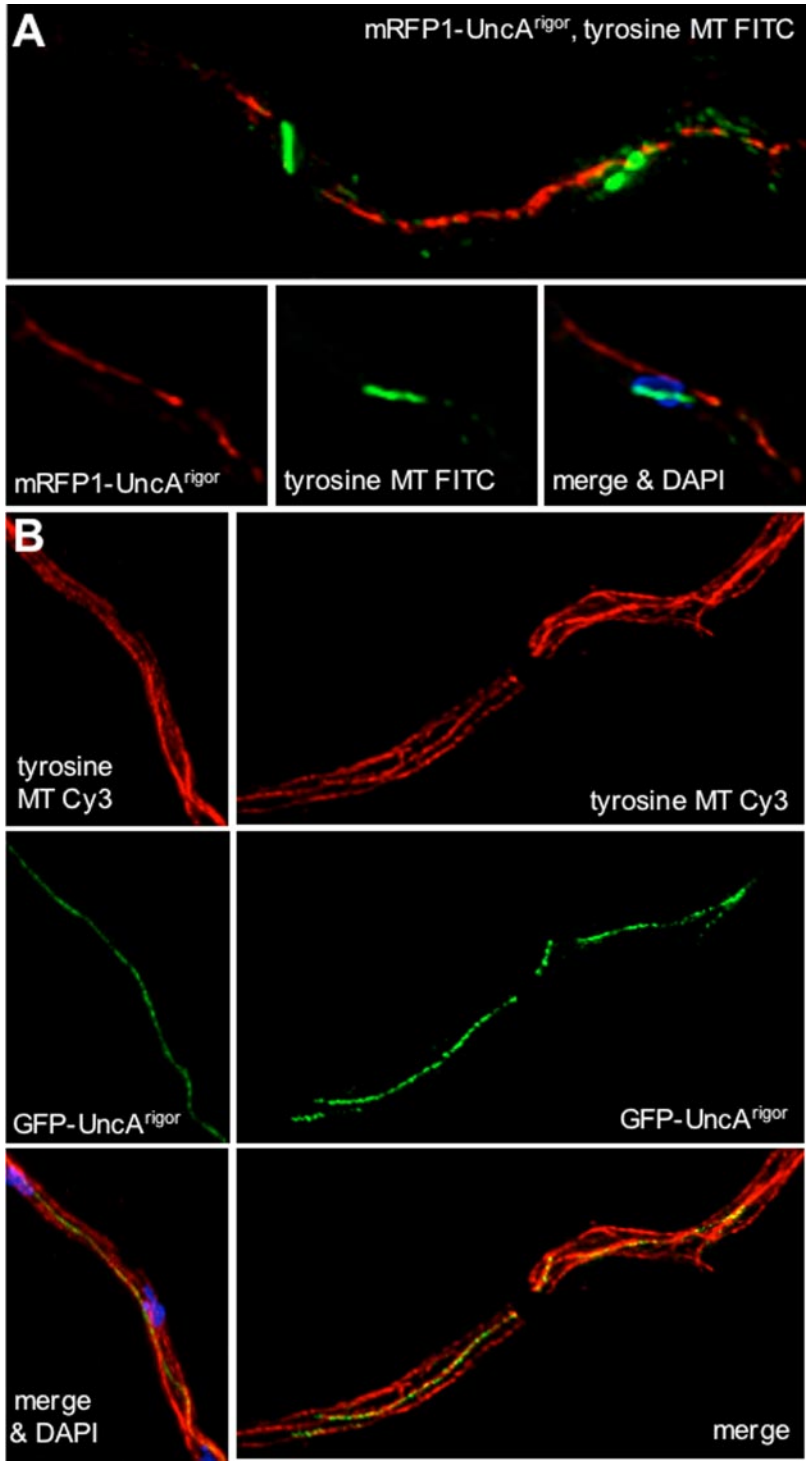

Figure 8. Immunostaining of mRFP1-UncA^{rigor} hyphae with anti-tyrosinated tubulin antibodies and FITC-labeled secondary antibodies. (A) Hyphal compartment during mitosis. mRFP1-UncA^{rigor} localizes to one MT in the cytoplasm but not to the two mitotic spindles, which are decorated with the green fluorescent FITC antibodies. The lower row of three pictures shows a second example and demonstrates that the anti-tyrosine antibody does not stain any microtubule in the cytoplasm (middle). Right, overlay of the mRFP1, FITC, and the DAPI channels. (B) Colocalization of GFP-UncA^{rigor} and tyrosinated microtubules (Cy3 stained) in interphase by laser scanning (left) and widefield fluorescence microscopy (right).

cargoes antero- and retrograde (Konzack *et al*., 2005). This mixed orientation of microtubule polarities is due to overlapping microtubules emanating from neighbor nuclei and in addition, from septa (Veith *et al*., 2005) (Figure 6). The effect of the deletion of conventional kinesin may be secondary, because KinA is required for dynein localization at the microtubule plus end (Zhang *et al*., 2003).

One most surprising result of this study was the finding that UncA moved preferentially along one microtubule. This was in contrast to other kinesins, which did not prefer any special microtubule. These findings suggest the existence of modified microtubules in *A. nidulans* and thereby most likely in other filamentous fungi. Already 30 years ago, a posttranslational modification at the C terminus of α-tubulin was detected in vertebrate brains (Arce *et al*., 1975). This modification was a RNA-independent incorporation of tyrosine. In most eukaryotes, the C terminus of α-tubulin is characterized by two glutamate residues followed by an aromatic amino acid such as tyrosine in mammals and phenylalanine in *S. cerevisiae*. The last amino acid is subjected to

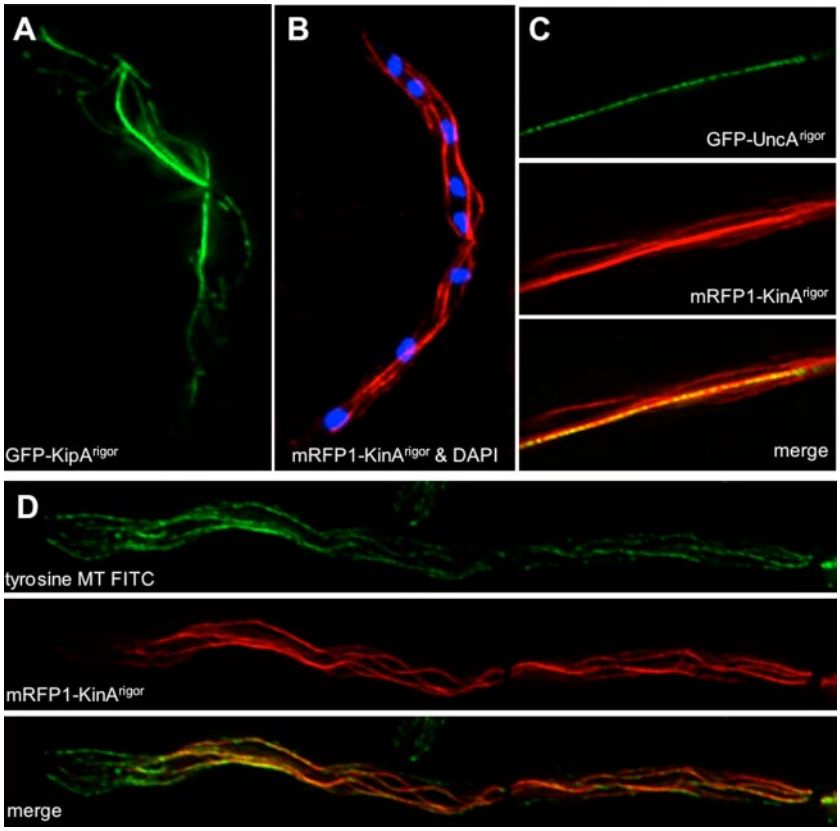

Figure 9. Comparison of the localization of three kinesin motor proteins in the rigor state. (A) GFP-KipA^{rigor}. (B) mRFP1-KinA^{rigor} overlaid with the DAPI channel. (C) Colocalization of GFP-UncA^{rigor} (top) with mRFP1-KinA^{rigor} (middle). Bottom, overlay. (D) Colocalization of mRFP1-KinA^{rigor} and tyrosinated microtubules in interphase. Top, FITC channel. Middle, mRFP channel. Bottom, overlay of the two channels.

a cyclic removal and readdition by a carboxypeptidase and a tubulin-tyrosin ligase. An equilibrium between the two modifying enzymes determines the status of the microtubule (Westermann and Weber, 2003). There is evidence that an accumulation of detyrosinated tubulin is associated with tumor growth (Mialhe *et al*., 2001). In *S. cerevisiae*, no cycling occurs, but detyrosinated microtubules are involved in nuclear oscillations (Badin-Larcon *et al*., 2004). Other modifications such as polyglutamylation, acetylation, and polyglycylation have not been reported in *S. cerevisiae* or filamentous fungi but in other eukaryotes including the most primitive eukaryote *Giardia lamblia* (Westermann and Weber, 2003). In this article, we showed that detyrosinated microtubules exist in *A. nidulans*, but we found no evidence for acetylated or polyglutamylated microtubules. To our knowledge, this is the first report of the existence of microtubule subpopulations in filamentous fungi.

There is increasing evidence that different modified microtubules play distinct roles in eukaryotic cells (Westermann and Weber, 2003). There was indirect evidence that Kif1A in mice binds preferentially to polyglutamylated microtubules (Ikegami *et al*., 2007). Our finding that UncA associated with detyrosinated microtubules is a second example for the specificity of kinesin-3 for certain microtubules and surprisingly, the specificity seems not to be evolutionarily conserved, given that the mice motor binds to polyglutamylated and the fungal one to detyrosinated microtubules. Another example for microtubule specificity was shown recently for conventional kinesin in neurites, where it binds preferentially to acetylated microtubules. Purified acetylated microtubules stimulated the kinesin activity (Reed *et al*., 2006). Furthermore, Dunn *et al*. (2007) found that kinesin-1 Kif5c binds preferentially to detyrosinated microtubules. In both cases these are stable microtubules. In summary, microtubule modifications seem to act as traffic signs for certain microtubule-dependent motor proteins. However, the exact cellular function for that is largely enigmatic and whether detyrosination has any effect on the UncA motor activity remains to be shown.

We found that modified microtubules are more stable but that the modification is not the cause but instead the consequence for the increased stability (Gundersen *et al*., 1984, 1987; Schulze *et al*., 1987). Likewise, we observed previously that some microtubules are not depolymerized as most microtubules are during mitosis of fast-growing hyphae (Veith *et al*., 2005). Indeed, in this study we found the GFP-UncA–labeled microtubule intact in the cytoplasm during nuclear division (Figure 10). This could be the reason for the evolution of the preference of the kin-3 motor in *A. nidulans*. If we assume that transportation of vesicles is important during all stages of the cell cycle; it would explain why the organism would have an advantage if the motor transporting them would preferentially bind to the one remaining stable during mitosis. Because vesicle movement is important for fast polarized growth, this stable microtubule could be important for the maintenance of hyphal extension during mitosis (Riquelme *et al*., 2003).

The question of microtubule modifications and their roles in vivo raises another very interesting question about the specificity of different motors. Motors thus are not only specific for their cargoes but also apparently also for their tracks. Further experiments in *A. nidulans* and other eukaryotes are required to better understand the biological importance of microtubule modifications and their interactions with molecular motors.

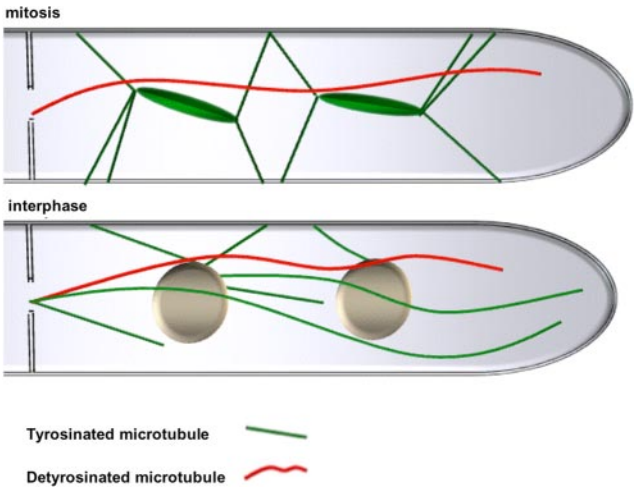

Figure 10. Proposed model for the arrangement of tyrosinated and detyrosinated microtubules during mitosis and during interphase in *A. nidulans*. For details, refer to *Discussion*.

ACKNOWLEDGMENTS

We thank Dr. Daniel Veith for contributions in the beginning of the project and Sabrina Hettinger for excellent technical assistance. This work was supported by the special program "Lebensmittel und Gesundheit" from the Landesstiftung of Baden-Württemberg and the Centre for Functional Nanostructures. N. Z. was partly supported with a fellowship of the Syrian Government.

REFERENCES

Aramayo, R., Adams, T. H., and Timberlake, W. E. (1989). A large cluster of highly expressed genes is dispensable for growth and development in *Aspergillus nidulans*. Genetics *122*, 65–71.

Araujo-Bazan, L., Peñalva, M. A., and Espeso, E. A. (2008). Preferential localization of the endocytic internalization machinery to hyphal tips underlies polarization of the actin cytoskeleton in *Aspergillus nidulans*. Mol. Microbiol. *67*, 891–905.

Arce, C. A., Rodriguez, J. A., Barra, H. S., and Caputo, R. (1975). Incorporation of L-tyrosine, L-phenylalanine and L-3,4dihydroxyphenylalanine as single units into rat brain tubulin. Eur. J. Biochem. *59*, 145–149.

Badin-Larcon, A. C., Boscheron, C., Soleilhac, J. M., Piel, M., Mann, C., Denarier, E., Fourest-Lieuvin, A., Lafanechère, L., Bornens, M., and Job, D. (2004). Suppression of nuclear oscillations in *Saccharomyces cerevisiae* expressing Glu tubulin. Proc. Natl. Acad. Sci. USA *101*, 5577–5582.

Basu, R., and Chang, F. (2007). Shaping the actin cytoskeleton using microtubule tips. Curr. Opin. Cell Biol. *19*, 1–7.

Dunn, S., Morrison, E. E., Liverpool, T. B., Molina-Paris, C., Cross, R. A., Alonso, M. C., and Peckham, M. (2007). Differential trafficking of Kif5c on tyrosinated and detryosinated microtubules in live cells. J. Cell Sci. *121*, 1085–1095.

Efimov, V., Zhang, J., and Xiang, X. (2006). CLIP-170 homologue and NUDE play overlapping roles in NUDF localization in *Aspergillus nidulans*. Mol. Biol. Cell *17*, 2021–2034.

Enke, C., Zekert, N., Veith, D., Schaaf, C., Konzack, S., and Fischer, R. (2007). *Aspergillus nidulans* Dis1/XMAP215 protein AlpA localizes to spindle pole bodies and microtubule plus ends and contributes to growth directionality. Eukaryot. Cell *6*, 555–562.

Fischer, R., Zekert, N., and Takeshita, N. (2008). Polarized growth in fungi—interplay between the cytoskeleton, positional markers and membrane domains. Mol. Microbiol. *68*, 813–826.

Fuchs, F., and Westermann, B. (2005). Role of Unc104/KIF1-related motor proteins in mitochondrial transport in *Neurospora crassa*. Mol. Biol. Cell *16*, 153–161.

Galagan, J. E. *et al*. (2005). Sequencing of *Aspergillus nidulans* and comparative analysis with *A. fumigatus* and *A. oryzae*. Nature *438*, 1105–1115.

Gundersen, G. G., Kalnoski, M. H., and Bulinski, J. C. (1984). Distinct populations of microtubules: tyrosinated and nontyrosinated alpha tubulin are distributed differently in vivo. Cell *38*, 779–789.

Gundersen, G. G., Khwaja, S., and Bulinski, J. C. (1987). Postpolymerization detyrosination of alpha-tubulin: a mechanism for subcellular differentiation of microtubules. J. Cell Biol. *105*, 251–264.

Hall, D. H., and Hedgecock, E. M. (1991). Kinesin-related gene *unc-104* is required for axonal transport of synaptic vesicles in *C. elegans*. Cell *65*, 837–847.

Hill, T. W., and Käfer, E. (2001). Improved protocols for *Aspergillus* minimal medium: trace element and minimal medium salt stock solutions. Fungal Genet. Newsl. *48*, 20–21.

Holthuis, J. C., Nichols, B. J., Dhruvakumar, S., and Pelham, H. R. (1998). Two syntaxin homologues in the TGN/endosomal system of yeast. EMBO J. *17*, 113–126.

Ikegami, K. *et al*. (2007). Loss of a-tubulin polyglutamylation in ROSA22 mice is assocated with abnormal targeting of KIF1A and modulated synaptic function. Proc. Natl. Acad. Sci. USA *104*, 3213–3218.

Klopfenstein, D. R., Tomishige, M., Stuurman, N., and Vale, R. D. (2002). Role of phosphatidylinositol(4,5)bisphosphate organisation in membrane transport by the Unc104 kinesin motor. Cell *109*, 347–358.

Konzack, S., Rischitor, P., Enke, C., and Fischer, R. (2005). The role of the kinesin motor KipA in microtubule organization and polarized growth of *Aspergillus nidulans*. Mol. Biol. Cell *16*, 497–506.

Kuratsu, M., Taura, A., Shoji, J.-Y., Kikuchi, S., Arioka, M., and Kitamoto, K. (2007). Systematic analysis of SNARE localization in the filamentous fungus *Aspergillus oryzae*. Fungal Genet. Biol. *44*, 1310–1323.

Lawrence, C. J. *et al*. (2004). A standardized kinesin nomenclature. J. Cell Biol. *167*, 19–22.

Lee, J., Shin, H., Choi, J., Ko, J., Kim, S., Lee, H., Kim, K., Rho, S., Lee, J., Song, H., Eom, S., and Kim, E. (2004). An intramolecular interaction between the FHA domain and a coiled coil negatively regulates the kinesin motor KIF1A. EMBO J. *23*, 1506–1515.

Meluh, P. B., and Rose, M. D. (1990). KAR3, a kinesin-related gene required for yeast nuclear fusion. Cell *60*, 1029–1041.

Mialhe, A. *et al*. (2001). Tubulin detyrosination is a frequent occurrence in breast cancers of poor prognosis. Cancer Res. *61*, 5024–5027.

Nakata, T., and Hirokawa, N. (1995). Point mutation of adenosine triphosphate-binding motif generated rigor kinesin that selectively blocks anterograde lysosome membrane transport. J. Cell Biol. *131*, 1039–1053.

Nayak, T., Szewczyk, E., Oakley, C. E., Osmani, A., Ukil, L., Murray, S. L., Hynes, M. J., Osmani, S. A., and Oakley, B. R. (2006). A versatile and efficient gene targeting system for *Aspergillus nidulans*. Genetics *172*, 1557–1566.

Okada, Y., and Hirokawa, N. (1999). A processive single-headed motor: kinesin superfamily protein KIF1A. Science *283*, 1152–1157.

Okada, Y., and Hirokawa, N. (2000). Mechanism of the single-headed processivity: diffusional anchoring between the K-loop of kinesin and the C terminus of tubulin. Proc. Natl. Acad. Sci. USA *97*, 640–645.

Okada, Y., Yamazaki, H., Sekine-Aizawa, Y., and Hirokawa, N. (1995). The neuron-specific kinesin superfamily protein KIF1A is a unique monomeric motor for anterograde axonal transport of synaptic vesicle precursors. Cell *81*, 769–780.

Otsuka, A. J., Jeyaprakash, A., García-Añoveros, J., Tang, L. Z., Fisk, G., Hartshorne, T., Franco, R., and Born, T. (1991). The *C. elegans unc-104* gene encodes a putative kinesin heavy chain-like protein. Neuron *6*, 113–122.

Pollock, N., deHostos, E. L., Turck, C. W., and Vale, R. D. (1999). Reconstitution of membrane transport powered by a novel dimeric kinesin motor of the Unc104/KIF1A family purified from *Dictyostelium*. J. Cell Biol. *147*, 493–506.

Reed, N. A., Dawen, C., Blasius, T. L., Jih, G. T., Meyhofer, E., Gaertig, J., and Verhey, K. J. (2006). Microtubule acetylation promotes kinesin-1 binding and transport. Curr. Biol. *16*, 2166–2172.

Requena, N., Alberti-Segui, C., Winzenburg, E., Horn, C., Schliwa, M., Philippsen, P., Liese, R., and Fischer, R. (2001). Genetic evidence for a microtubule-destabilizing effect of conventional kinesin and analysis of its consequences for the control of nuclear distribution in *Aspergillus nidulans*. Mol. Microbiol. *42*, 121–132.

Riquelme, M., Fischer, R., and Bartnicki-Garcia, S. (2003). Apical growth and mitosis are independent processes in *Aspergillus nidulans*. Protoplasma *222*, 211–215.

Rischitor, P., Konzack, S., and Fischer, R. (2004). The Kip3-like kinesin KipB moves along microtubules and determines spindle position during synchronized mitoses in *Aspergillus nidulans* hyphae. Eukaryot. Cell *3*, 632–645.

Rivera, S. B., Koch, S. J., Bauer, J. M., Edwards, J. M., and Bachand, G. D. (2007). Temperature dependent properties of a kinesin-3 motor protein from *Thermomyces lanuginosus*. Fungal Genet. Biol. *44*, 1170–1179.

Sambrook, J., and Russel, D. W. (1999). Molecular Cloning: A Laboratory Manual, Cold Spring Harbor, New York: Cold Spring Harbor Laboratory Press.

Schliwa, M., and Woehlke, G. (2003). Molecular motors. Nature *422*, 759–765.

Schoch, C. L., Aist, J. R., Yoder, O. C., and Turgeon, B. G. (2003). A complete inventory of fungal kinesins in representative filamentous ascomycetes. Fungal Genet. Biol. *39*, 1–15.

Schuchardt, I., Aßmann, D., Thines, E., Schuberth, C., and Steinberg, G. (2005). Myosin-V, kinesin-1, and kinesin-3 cooperate in hyphal growth of the fungus *Ustilago maydis*. Mol. Biol. Cell *16*, 5191–5201.

Schulze, E., Asai, D. J., Bulinski, J. C., and Kirschner, M. (1987). Posttranslational modification and microtubule stability. J. Cell Biol. *105*, 2167–2177.

Seiler, S., Nargang, F. E., Steinberg, G., and Schliwa, M. (1997). Kinesin is essential for cell morphogenesis and polarized secretion in *Neurospora crassa*. EMBO J. *16*, 3025–3034.

Song, Y.-H., Marx, A., Müller, J., Woehlke, G., Schliwa, M., Krebs, A., Hoenger, A., and Mandelkow, E. (2001). Structure of a fast kinesin: implications for ATPase mechanism and interactions with microtubules. EMBO J. *20*, 6213–6225.

Steinberg, G. (2007). On the move: endosomes in fungal growth and pathogenicity. Nat. Rev. Microbiol. *5*, 309–316.

Stringer, M. A., Dean, R. A., Sewall, T. C., and Timberlake, W. E. (1991). *Rodletless*, a new *Aspergillus* developmental mutant induced by directed gene inactivation. Genes Dev. *5*, 1161–1171.

Suelmann, R., and Fischer, R. (2000). Mitochondrial movement and morphology depend on an intact actin cytoskeleton in *Aspergillus nidulans*. Cell Motil. Cytoskeleton *45*, 42–50.

Taheri-Talesh, N., Horio, T., Araujo-Bazan, L., Dou, X., Espeso, E. A., Penalva, M. A., Osmani, A., and Oakley, B. R. (2008). The tip growth apparatus of *Aspergillus nidulans*. Mol. Biol. Cell (*in press*).

Takeshita, N., Higashitsuji, Y., Konzack, S., and Fischer, R. (2008). Apical sterol-rich membranes are essential for localizing cell end markers that determine growth directionality in the filamentous fungus *Aspergillus nidulans*. Mol. Biol. Cell *19*, 339–351.

Toews, M. W., Warmbold, J., Konzack, S., Rischitor, P. E., Veith, D., Vienken, K., Vinuesa, C., Wei, H., and Fischer, R. (2004). Establishment of mRFP1 as fluorescent marker in *Aspergillus nidulans* and construction of expression vectors for high-throughput protein tagging using recombination in *Escherichia coli* (GATEWAY). Curr. Genet. *45*, 383–389.

Upadhyay, S., and Shaw, B. D. (2008). The role of actin, fimbrin and endocytosis in growth of hyphae in *Aspergillus nidulans*. Mol. Microbiol. *68*, 690–705.

Veith, D., Scherr, N., Efimov, V. P., and Fischer, R. (2005). Role of the spindle-pole body protein ApsB and the cortex protein ApsA in microtubule organization and nuclear migration in *Aspergillus nidulans*. J. Cell Sci. *118*, 3705–3716.

Waring, R. B., May, G. S., and Morris, N. R. (1989). Characterization of an inducible expression system in *Aspergillus nidulans using alcA* and tubulin coding genes. Gene *79*, 119–130.

Wedlich-Söldner, R., Straube, A., Friedrich, M. W., and Steinberg, G. (2002). A balance of KIF1A-like kinesin and dynein organizes early endosomes in the fungus *Ustilago maydis*. EMBO J. *21*, 2946–2957.

Westerholm-Parvinen, A., Vernos, I., and Serrano, L. (2000). Kinesin subfamily UNC104 contains a FHA domain: boundaries and physicochemical characterization. FEBS Lett. *486*, 285–290.

Westermann, S., and Weber, K. (2003). Post-translational modifications regulate microtubule function. Nat. Rev. Mol. Cell Biol. *4*, 938–947.

Wickstead, B., and Gull, K. (2006). A "Holistic" kinesin phylogeny reveals new kinesin families and predicts protein functions. Mol. Biol. Cell *17*, 1734–1743.

Xiang, X., Roghi, C., and Morris, N. R. (1995). Characterization and localization of the cytoplasmic dynein heavy chain in *Aspergillus nidulans*. Proc. Natl. Acad. Sci. USA *92*, 9890–9894.

Yelton, M. M., Hamer, J. E., and Timberlake, W. E. (1984). Transformation of *Aspergillus nidulans* by using a *trpC* plasmid. Proc. Natl. Acad. Sci. USA *81*, 1470–1474.

Zhang, J., Li, S., Fischer, R., and Xiang, X. (2003). The accumulation of cytoplasmic dynein and dynactin at microtubule plus-ends is kinesin dependent in *Aspergillus nidulans*. Mol. Biol. Cell *14*, 1479–1488.

INCYTES from MBC
January, Vol. 20, Nos. 1 and 2

Sterols Are Mainly in the Cytoplasmic Leaflet of the Plasma Membrane and the Endocytic Recycling Compartment in CHO Cells

Mousumi Mondal, Bruno Mesmin, Sushmita Mukherjee, and Frederick R. Maxfield

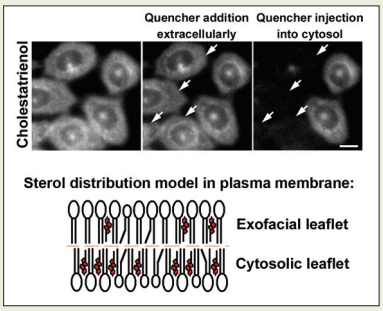

Transbilayer asymmetry is a general feature of most lipids in the plasma membrane and other post–endoplasmic reticulum organelles. This asymmetry has important consequences for membrane physical properties and cell signaling. Although cholesterol is a major lipid in these membranes, its transbilayer distribution is not well understood. Using fluorescent sterols (dehydroergosterol and cholestatrienol) and a variety of fluorescence quenchers, the authors determined that the majority of sterol is in the cytoplasmic leaflet of the plasma membrane and endocytic recycling compartment of CHO cells. Quenchers that are restricted to the exofacial leaflet of the plasma membrane reduce the fluorescence intensity by about 20%–30%, whereas microinjection of quenchers into the cytosol quenched the fluorescent sterols associated with the plasma membrane and endocytic recycling compartment by about 60%. The presence of high amounts of cholesterol in the cytoplasmic leaflet might have important implications for intracellular cholesterol transport and for membrane domain formation.

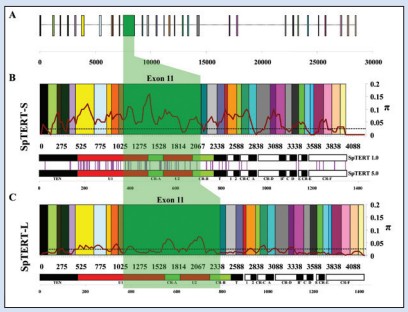

Genetic Hypervariability in Two Distinct Deuterostome Telomerase Reverse Transcriptase Genes and Their Early Embryonic Functions

Trystan B. Wells, Guanglei Zhang, Zenon Harley, and Homayoun Vaziri

Within a species of complex animals, genes for functional proteins are rarely variant. This constancy is thought to be required for the function of essential proteins. One such crucial protein is telomerase reverse transcriptase catalytic subunit (TERT). To study the function of TERT during early development, the authors cloned *SpTERT* from purple sea urchin embryos. Unexpectedly, they discovered two distinct telomerase genes named *SpTERT-S* and *SpTERT-L*. By cloning SpTERT from several individuals, they further discovered regions, especially exon 11 of *SpTERT-S*, with intraspecific germline hypervariability. Although the variant enzymes remained catalytically active, there were significant amino acid variations in multiple regions, including those involved in binding of TERT to its RNA component. The authors also uncovered a noncanonical essential function for telomerase that is required for embryo polarity at the mesenchymal blastula stage. These results suggest the presence of an active diversity-generation mechanism that has neofunctionalized telomerase throughout evolution.

The *Aspergillus nidulans* Kinesin-3 UNCa Motor Moves Vesicles along a Subpopulation of Microtubules

Nadine Zekert and Reinhard Fischer

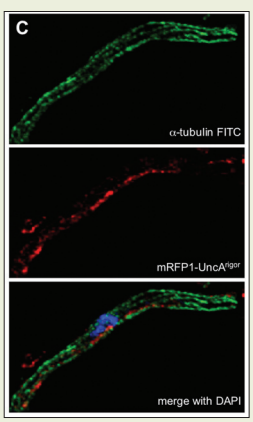

The microtubule cytoskeleton is not as rigid and uniform as the name implies, but is characterized by its dynamic instability. In addition, microtubules can be made up of different tubulin isoforms and—to make a eukaryotic cell even more complex—of different posttranslationally modified tubulins. Microtubule modifications, such as acetylation or polyglutamylation, are evolutionarily old "inventions" and occur in primitive eukaryotes such as *Giardia lamblia,* whereas detyrosination appeared later during evolution. Although many modifications were discovered more than 20 years ago, their cellular functions are not well understood. Here, the authors show that in the filamentous fungus *Aspergillus nidulans* at least two different microtubule populations exist. This discovery came from studies of an unc-104–related motor protein that preferentially moves along detyrosinated microtubules and transports vesicles. These microtubules are more stable than the tyrosinated ones and even remain intact during mitosis when other cytoplasmic microtubules are degraded.

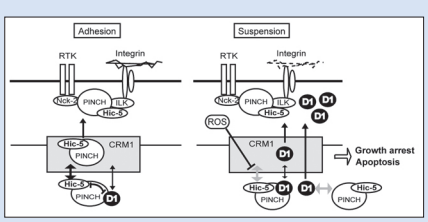

Competitive Nuclear Export of Cyclin D1 and Hic-5 Regulates Anchorage Dependence of Cell Growth and Survival

Kazunori Mori, Etsuko Hirao, Yosuke Toya, Yukiko Oshima, Fumihiro Ishikawa, Kiyoshi Nose, and Motoko Shibanuma

Anchorage dependence of cell growth is a critical trait that distinguishes nontransformed from transformed cells. The authors report a novel mechanism whereby anchorage-independent cell growth and survival is prevented. Cyclin D1 is a proto-oncogene that exhibits cell cycle– dependent nuclear localization. Its nuclear export is dependent on CRM1. The authors report that the nuclear localization of cyclin D1 is adhesion-dependent and regulated by the focal adhesion protein Hic-5 and its binding partner PINCH, which also cycle in and out of the nucleus. Hic-5 binds to CRM1 with high affinity and is a competitive inhibitor of CRM1-dependent cyclin D1 export in adherent cells. PINCH interacts with both cyclin D1 and Hic-5 and enhances the Hic-5–dependent inhibition of cyclin D1 export. Under nonadherent conditions, the cellular level of reactive oxygen species increases and inhibits the nuclear export of Hic-5, resulting in the nuclear export of cyclin D1. Consequently cells undergo growth arrest and apoptosis. *Ras* overexpression led to the anchorage-independent nuclear localization of cyclin D, revealing an interesting interdependence of the oncogenic potential of two oncogenes. ■